International Research Journal of Innovations in Engineering and Technology (IRJIET)

ISSN (online): 2581-3048
Volume 7, Issue 3, pp 36-49, March-2023
https://doi.org/10.47001/IRJIET/2023.703006

Major Role of Annealing Temperature Effect on the Structural Pathways, Optical Properties, Sheet Resistance, Quality Factor, and Electronic Parameters of Selenium-Rich $Ge_{15}Se_{85}$ Pristine Thin Film for Optoelectronic Applications

[1]Mehdi Ahmed Dabban, [2]Tawfik Mahmood Mohammed Ali, [3]Abdel-naser A. M. Alfaqeer

[1]Associate Professor, Physics Department, Faculty of Science, University of Aden, Yemen
[2]Associate Professor, Physics Department, Faculty of Education, University of Aden, Yemen
[3]Associate Professor, Physics Department, Faculty of Science and Education, Saba Region University, Yemen

***Abstract* - A thin film's microstructural and optical properties are essential for the development of optoelectronic devices. As a result, the thermal evaporation of selenium-rich $Ge_{15}Se_{85}$ (SR-GeSe with thickness of 250 *nm*) thin films was investigated for improving these properties. The films fabricated in a pure nitrogen-rich atmosphere were annealed in the thermal temperature range between 200°C and 300°C for 30 minutes. The microstructural, compositional, and optical characteristics of these films were investigated using X-ray diffraction (XRD), scanning electron microscopy (SEM) coupled with the energy dispersive X-ray analysis (EDXA), and UV-Vis-INR spectrophotometers. In accordance with the XRD patterns, the as-prepared films were in an amorphous state, while the annealed films were in the polycrystalline style. In annealed films, crystalline phases with hexagonal orientations were formed. Crystallographic parameters were significantly affected by thermally induced effects. As seen from the surface morphology, the films were nearly densely packed, homogeneous, smooth, uniform, and free from holes and voids. In the thin films of SR-GeSe, the band gap and Urbach energies behaved oppositely. Amorphous-crystalline transitions and the Mott-Davis model were used to explain the studied optical properties. The single oscillator for Wimple-DiDomenico (WDD) model described the refractive index scattering whose parameters were determined as a function of annealing temperature. By adjusting the thermal annealing process, the microstructural and optical properties of SR-GeSe thin films were improved, indicating their suitability for thermo-optic applications. On the other side, the electronic parameters including the energies of Plasmon, Penn, Fermi and the number of active electrons were computed.**

Keywords: SR-GeSe thin films, Microstructural pathways, Optical parameters, Optical constants, Electronic parameters.

I. INTRODUCTION

The potential applications of chalcogenide glasses in various solid-state technologies have received much attention in the technology field [1-4].These materials, especially those based on selenium, had applications in blue-colored laser diodes, as an amplifier for optical signals, in the field of dry and laser imaging for peace and war purposes, solar cells and optical lithography, as well as optical fibers that carry signals over long distances [5-11]. On the other hand, amorphous Germanium Selenide (GeSe) thin films have been exploited in smart memory systems, giant screens, and signal switching devices due to their many advantages, including the wide range of optical transmission over a wide spectral region extending to the near-infrared region, in addition to the general structural stability of the properties under normal conditions and thermal stability [12-14].

It is expected that thermal annealing will significantly influence chalcogenide glasses' microstructural pathways, transport processes, optical properties, and practical applications. Germanium Selenide systems have not been sufficiently studied for their growth, properties, and characterization. A previous study by Baker *et al.* [15] investigated the structural characteristics of Ge_xSe_{1-x} thin films synthesized using the semi-closed space technique where x was in the range of (0.1-0.5 *wt.*%). Amorphous state and maximal glass transition temperatures were determined by X-rays and DTA measurements at x~0.28. At this content (x=0.28), the measured band-gap energy increased at its maximum value while the tail width reached its maximum value at $0.2 < x < 0.32$. Alnajjar studied heat treatments of

International Research Journal of Innovations in Engineering and Technology (IRJIET)

ISSN (online): 2581-3048

Volume 7, Issue 3, pp 36-49, March-2023

https://doi.org/10.47001/IRJIET/2023.703006

$Ge_{0.15}Se_{0.85}$ thin films in the range of (25-177°C) [16]. As the annealing temperature increased, the energy gap E_g increased and the absorption edge moved to shorter wavelengths as a result according to the mentioned study.

Meshal, *et al.*[6] studied the $Ge_{20+x}Se_{80-x}$ thin films synthesized using the thermally evaporation technique at the corresponding conditions (25°C, the layer thickness of 890 *nm*, different contents of *x* ranges from 5 to 30 at.%). Using only the wavelength measurements of the normal and slightly slanted incident light, the real optical constant and film thickness of GeSe thin films have been estimated in this study. It was decided on the optical parameters, optical constants, and dispersion parameters. The placements of the energy states and the optical dispersion, (phase & group velocities), magneto-optical constant have all been well examined. An effect of microwave radiation and thermal annealing temperatures on the optical properties and structural properties of Ge25Se75 thin films was recently investigated [17, 18]. As illumination time or thermal annealing temperature increases, they observed amorphous-crystalline transitions and increased optical band gaps.

The objective of this study was to investigate the microstructure and surface morphology changes of the $Ge_{15}Se_{85}$ thin films that were prepared by thermal evaporation, called selenium-rich GeSe (SR-GeSe) thin films. For annealed films, crystallite size, micro-strain, and dislocation density were determined from XRD data. In addition, thermally evaporated SR-GeSe thin films were investigated to know spectral behavior, optical constants, and dispersion parameters at different temperatures (25°-300°C). The parent material was a melt-quenched $Cd_{15}Se_{85}$ alloy. SR-GeSe thin films have been studied only in limited works, so the findings in this work are likely to be valuable to future researchers in the field of chalcogenide glasses. Electronic parameters of optical materials are important because they are applied in a wide range of applications, such as solar cells, optical sensors, detectors, diodes, optical filters, display screens, alarm systems, photoelectric circuits, etc. For this reason, several electronic parameters have been addressed, and we documented the relationship between the refractive index and the optical bandgap energy in this work.

II. THEORETICAL BACKGROUND

In the polycrystalline films, an estimate of the average crystallite size based on the Scherrer's formula $D = 0.94(\lambda/\beta\cos\theta)$ [19], the residual strain $\varepsilon = (\tan\theta)^{-1}.\left[\lambda.(D.\cos\theta)^{-1} - \beta\right]$ [20, 21] and the length of dislocation lines per unit volume (the dislocation density $\delta = (d \times D^{-3})$)[21] are also computed via X-ray diffraction. In the mentioned formula, *d* is the film's thickness, β (or FWHM) portrays the full width at half maximum (in radian unit), θ is the Bragg's angle in the range of (4°-90°) and λ=1.5418 Å for the CuK_α radiation.

The band tails (E_e), which represent the formed localized states near the band edges, can be used to measure the degree of disorder in an amorphous semiconductor. This energy computes using Urbach's formula $\alpha(\nu) = \alpha_o \exp(h\nu / E_e)$ [19], where *h* in this formula refers to Plank's constant, *hv* represents the photon energy in the range of (300-2500 *nm*), α_o is constant and $\alpha(\nu)$ is the absorption coefficient determined via the following formula in terms of optical spectra [transmittance, *T*(λ)& reflectance *R*(λ) and the film's thickness *d*] [20]:

$$\alpha = d^{-1}.\ln\left[(1-R)^2 \times (2T)^{-1} + \left\{\left((1-R)^2 \times (2T)^{-1}\right)^2 - R^2\right\}^{0.5}\right] \quad (1)$$

The second important optical parameter in this study is the optical bandgap energy, E_g -Tauc energy- which in turn is calculated according to the following equation [22]:

$$\alpha h\nu = A\left(h\nu - E_g\right)^r \quad (2)$$

A is the edge width parameter indicating the film quality; *r* indicates the allowed or forbidden status of direct or indirect transitions.

On the other pathway, the linear optical constants (the refractive index is:

$n = (1+R)/(1-R) + \left[\left[(1+R)/(1-R)\right]^2 - (1+k_{ex}^2)\right]^{0.5}$, and the extinction coefficient is $k = \alpha\lambda/4\pi$ [22], the real dielectric constant $\varepsilon_r = n^2 - k_{ex}^2$ [23] and imaginary dielectric part $\varepsilon_i = 2nk$ are very important in optoelectronic applications.

A high-frequency dielectric constant ε_∞ has been computed using Drude's theory, which takes into account both free carriers and lattice vibration modes of dispersion [24, 25], according to the following formula:

$$\varepsilon_r = \tilde{n}^2 = \varepsilon_\infty - \left(\frac{e^2 N}{4\pi^2 c^2 \varepsilon_o m^*}\right)\lambda^2 \quad (3)$$

In this equation,*e* represents the electronic charge which equal 1.6 x 10^{-19} C, *c* is the light velocity (3x10^8 m/sec), $\varepsilon_o$portrays the free space dielectric constant (8.845×10^{-12}*F/m*),

International Research Journal of Innovations in Engineering and Technology (IRJIET)

ISSN (online): 2581-3048

Volume 7, Issue 3, pp 36-49, March-2023

https://doi.org/10.47001/IRJIET/2023.703006

N and m^* are the free carrier concentration and its effective mass, respectively [25]. In addition, the plasma resonance frequency ω_p is calculated now easy from the following equation [26, 27]:

$$\omega_p = \sqrt{\left(\frac{e^2}{\varepsilon_o \varepsilon_\infty}\right) / \frac{N}{m^*}} \tag{4}$$

Based on the single oscillator model proposed by Wemple and Didomenico, the refractive index values below the interband absorption edge $n^2 = 1 + E_d E_o . \left[E_o{}^2 - (h\nu)^2\right]^{-1}$ were analyzed to extract the dispersion parameters (the single oscillator constant E_o, and dispersion energy E_d) [28, 29].

After knowing the plasma frequency, an important set of parameters can be easily extracted, called electronic parameters, and they include Plasmon, Penn, and Fermi energies, (Ψ , E_p and E_F) which are computed according to the following equations [30, 31]:

$$\left.\begin{aligned} \Psi &= \hbar\omega_p = (h/2\pi).\omega_p \\ E_P &= \Psi \Big/ \sqrt{(\varepsilon_\infty - 1)} \\ E_F &= 0.3 \times \sqrt[3]{\Psi^4} \end{aligned}\right\} \tag{5}$$

In the related side, the total effective count of valence electrons n_{eff} is extracted according the following [30]:

$$\left.\begin{aligned} n_{eff} &= 0.12.(\Psi^2 \times V_m),\ V_m = \frac{M}{\rho} \\ M &= \left(\frac{(15 \times M_{Ge}) + (85 \times M_{Se})}{100}\right) \\ \rho &= \left(\frac{(15 \times \rho_{Ge}) + (85 \times \rho_{Se})}{100}\right) \end{aligned}\right\} \tag{6}$$

Here, V_m is the molar volume, ρ portrays the density of studied composition (with unit of g/cm^3) and M represents the molecular weight (with unit of g/mol.).

The electronic polarization α_p in terms of the three mentioned energies is computed from the following formula [32-34]:

$$\alpha_p = (0.4 \times 10^{-24}).\left(\frac{(\Psi)^2.[1 - (\frac{E_P}{4E_F}) + \frac{1}{3}(\frac{E_P}{4E_F})^2]}{(\Psi)^2[1 - (\frac{E_P}{4E_F}) + \frac{1}{3}(\frac{E_P}{4E_F})^2] + 3E_P^2}\right) \times V_m \tag{7}$$

Reddy *et al.* [35] proposed the following empirical formulas to extract the electronic polarization in terms of the optical band gap:

$$\alpha_p = \left(0.4 \times 10^{-24}\right).\left(\frac{(12.41 - \sqrt{E_g - 0.365})}{(12.41 + 2\sqrt{E_g - 0.365})}\right) \times V_m \tag{8}$$

$$\alpha_p = 0.4 \times 10^{-24}\left(\frac{(5.563 - \left[0.033 \times 168.58 + 30.3\ln(0.027E_g)\right])^2 - 1}{(5.563 - \left[0.033 \times 168.58 + 30.3\ln(0.027E_g)\right])^2 + 2}\right) \times V_m \tag{9}$$

$$\alpha_p = (0.4 \times 10^{-24}) \times \left(\frac{4.06 - \sqrt{E_g}}{4.06}\right) \times V_m \tag{10}$$

In terms of ε_∞, α_p is computed based on the Clausius-Mossotti Model (CMM) as follows [36]:

$$\alpha_p = \left(0.4 \times 10^{-24}\right) \times \left(\frac{(\varepsilon_\infty - 1)}{(\varepsilon_\infty + 2)}\right) \times V_m \tag{11}$$

The path followed by the refractive index of the studied thin films can be traced with the knowledge of the optical bandgap energy according to the following equations, according to the proposal of several scientists:

Tripathy, $n(T)$ [37]:

$$n(T) = 1.73 + \left[\left(3.28 \times \exp - (0.54 \times E_g)\right)\right] \tag{12}$$

Moss, $n(M)$ [38]:

$$n(M) = 3.12/\sqrt[4]{E_g} \tag{13}$$

Ravindra, $n(R)$ [39]:

$$n_R = 4.08 - [0.62 \times E_g] \tag{14}$$

Herve-Vandamme, $n(HV)$ [40, 41]:

$$n(HV) = \sqrt{\left(1 + \frac{184.96}{(E_g + 3.47)^2}\right)} \tag{15}$$

International Research Journal of Innovations in Engineering and Technology (IRJIET)

ISSN (online): 2581-3048

Volume 7, Issue 3, pp 36-49, March-2023

https://doi.org/10.47001/IRJIET/2023.703006

Reddy and Anjaneyulu, $n(RA)$ [42]:

$$n(RA) = 3.6 - \ln(E_g) \quad (16)$$

Gupta and Ravindra, $n(GR)$ [43]:

$$n(GR) = 4.16 - 1.12E_g + 0.31E_g^2 - 0.08E_g^3 \quad (17)$$

Kumar and Singh, $n(KS)$ [38]:

$$n(KS) = \frac{3.367}{E_g^{0.32}} \quad (18)$$

III. EXPERIMENTAL DETAILS

The first step in preparing the bulk material in any system formed as an ingot (alloy) is to use the melt cooling melt quenching technique (melt quenching process). In our studied system, the alloy was in the form of a mixture that combines selenium with germanium, which is of high purity at an estimated rate of 99.999%, as they were purchased from (Aldrich Chem. Co, USA), and for this combination, the corresponding structural formula: $Ge_{15}Se_{85}$ (SR-GeSe) was prepared according to the aforementioned method. These components were weighed using an electrically sensitive scale with 0.1 mg accuracy.

To ensure a high level of uniformity and homogeneity for the final alloy, we prepared the weighted elements in an evacuated (10^{-5}Torr), silica tube at 950°C for 26 hours in a furnace that vibrates regularly during the synthesis process. An ice-cold water bath was used to cool the molten substance after synthesis. Thermal evaporation was used to deposit thin films on clean glass substrates in an easily-rotatable holder. The films were all deposited at room temperature. Rotation speed resulted in a homogeneous film thickness distribution of around 250 *nm*. During film deposition process, the Edward Coating Unit (ECU-306A) vacuum chamber was pumped down to (10^{-5} Torr). The film thickness was determined using quartz crystal thickness monitor (FTMS). The samples were annealed for 30 minutes under pure nitrogen flow in a Pyrex tube furnace at 200-300°C to prevent oxidation.

In order to obtain the XRD data, a Philips diffractometer, PW1710-Model, was used, and it was equipped with a copper target with a wavelength of 1.5418 Å, and at the other end it was equipped with a nickel filter. Measurement by this device gave an accurate description of the structure of the pristine thin film and the annealed thin films. In this study, the composition of GeSe powder material was determined by energy dispersive X-ray analysis (EDXA), coupled to a Jeol (JSM)-T200 type scanning electron microscope (SEM).

In order to examine the surface morphology of the films using SEM, they were coated with gold prior to examination. The transmittance, *T(λ)*, and reflectance, *R(λ)*, of the films deposited on glass substrates, were measured optically at normal incidence in the wavelength range of (300-2500*nm*) using a double-beam spectrophotometer (JASCO-570) connected to a specular reflection stage.

III. RESULTS AND DISCUSSIONS

3.1 Structural Pathways: (EDXA, XRD and SEM)

SR-GeSe materials in bulk form were experimentally examined using EDXA. It was found that Ge and Se actually had elemental ratios that were close to the original ratios. The constituent element ratio of the examined thin films was 14.56:85.44*wt.*%, which is comparable to the expected compositions as indicated in Fig.1 (a).The X-ray diffraction patterns of annealed SR-GeSe thin films were investigated to determine the crystalline phases. The XRD patterns of the pristine and annealed SR-GeSe thin films are given in Fig.1 (b). The absence of distinct sharp structural peaks in these patterns confirmed the amorphous nature (glassy stage) of the thin film as it was formed.

Amorphous to crystalline phase transition was confirmed by the polycrystalline structure of thin films after 30 minutes of annealing for the annealed samples from 240°C to 300°C. The study of XRD patterns from all annealed samples reveals that $GeSe_2$ and Se are the major crystalline phases. The interplanar spacing (d_{cal}) was calculated using Bragg's formula ($d_{cal}=\lambda/2\sin\theta$) where θ is Bragg's angle, λ is the wavelength of the used X-ray. The calculated values of d_{cal} for annealed thin films are in good agreement with the standard JCPDS values d_{stand} for Se and $GeSe_2$ phases.

The intensity of the peaks grew when the annealing temperature was raised, indicating a significant rise in the volume fraction of two crystalline phases. Via the XRD patterns the average crystallite size, strain, and dislocation density of fresh and annealed samples according to formulas in the theoretical section were determined. The computed values of these variables are provided in Table 1. When the annealing temperature is raised, it is seen that the strain and dislocation density for the $GeSe_2$ and Se phases decrease while the average crystallite size increases. This means that the films' crystallization has improved.

International Research Journal of Innovations in Engineering and Technology (IRJIET)

ISSN (online): 2581-3048

Volume 7, Issue 3, pp 36-49, March-2023

https://doi.org/10.47001/IRJIET/2023.703006

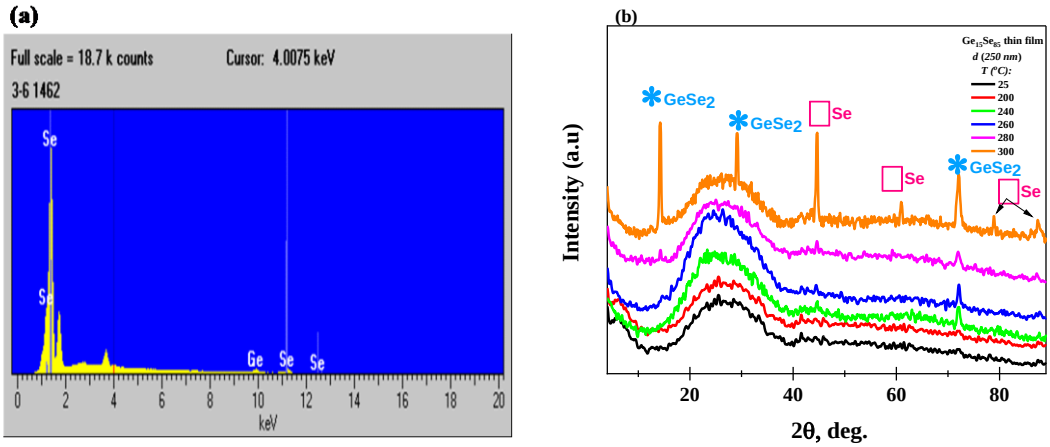

Figure 1(a,b): Mapping of EDXA And XRD Pathways for Pristine and Annealed SR-GeSe Thin Films

Table 1: Structural Parameters of the Last Four Annealed SR-GeSe Thin Films

T (°C)	Phases	(h k l)	$d_{cal.}$ (Å)	$d_{stand.}$ (Å)	D(nm)	ε × 10-3 ($lin^{-2}.m^{-4}$)	δ× 1014 ($lines/m^2$)	No. Card
240	$GeSe_2$	(315)	1.31	1.308	20	2.08	24.5	16-0080
260	$GeSe_2$	(315)	1.309	1.308	24	1.9	22	16-0080
280	$GeSe_2$	(020)	6.18	6.15	26	1.8	19	16-0080
	$GeSe_2$	(315)	1.311	1.308				33-0581
	Se	(314)	2.029	2.025	22	1.7	20	85-0566
300	$GeSe_2$	(020)	6.208	6.150	27	1.6	18.5	16-0080
	$GeSe_2$	(105)	3.056	3.040				33-0581
	$GeSe_2$	(315)	1.309	1.308				04-003-4149
	Se	(314)	2.029	2.025	29	1.5	16	85-0566
	Se	(103)	1.519	1.515				83-2438

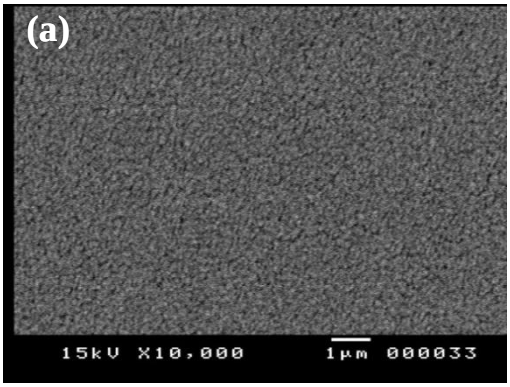

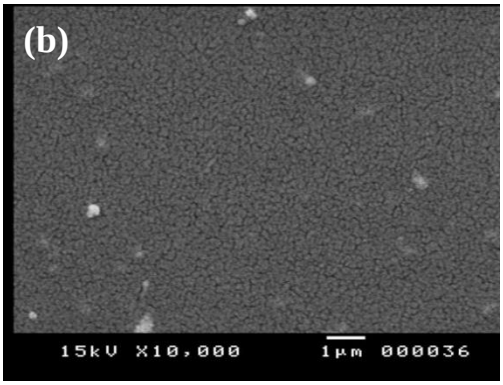

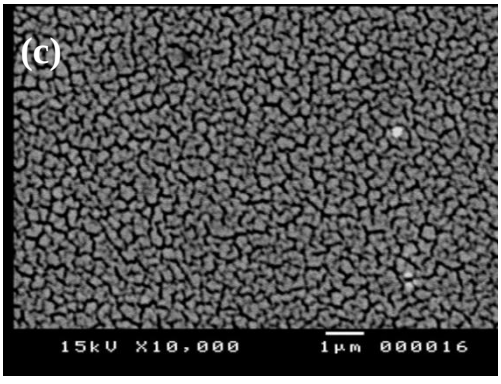

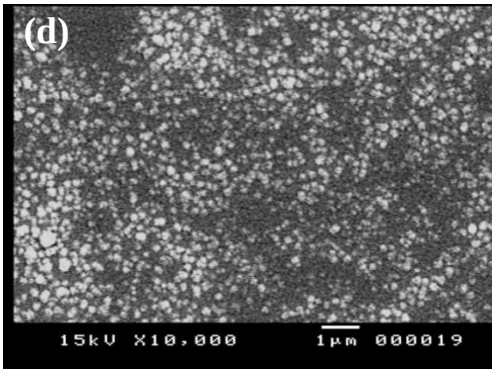

International Research Journal of Innovations in Engineering and Technology (IRJIET)

ISSN (online): 2581-3048

Volume 7, Issue 3, pp 36-49, March-2023

https://doi.org/10.47001/IRJIET/2023.703006

Figure 2: SEM Micrographs For SR-GeSe Thin Films: (A) Pristine (B) Annealed at 240˚C, (C) Annealed at 260˚C And (D) Annealed at 300˚C

Fig. 2 (a-d) displays a top view of SEM image for SR-GeSe pristine and annealed thin films. The surface morphology of annealed thin film illustrated in Fig. 2 (b-d) exhibits tiny semispherical crystallites uniformly scattered over smooth, homogeneous backdrop, in contrast to the pristine image of the thin film displayed in Fig. 2 (a), which offers a fully amorphous matrix without any discernible agglomerations. When the annealing temperature is increased from 240˚C to 300 ˚C, the crystallites become clearer and larger. This supports the findings of crystallite size calculations based on XRD patterns. This improvement in the size of the crystals in particular and the structural properties in general will result in an improvement in the optical and electrical properties [27, 32].

3.2 Optical Analysis

The transmission $T(\lambda)$ and reflection $R(\lambda)$ in the wavelength range of (300–2500 *nm*) for pristine and annealed SR-GeSe thin films are illustrated in Fig. 3(a,b). Between 500 and 1000 *nm* in the Vis-NIR spectral region, there is a maximum in transmission and a minimum in reflection pathways. Values of the maximum and minimum pathways can be associated with one another. As annealing temperature rises, transmittance normally falls while the reflectance spectrum shows the opposite tendency. However, the optical absorption coefficient (α) was determined from the experimentally measured transmission $T(\lambda)$ and reflection $R(\lambda)$ values of SR-GeSe thin films. The relationship between the absorption coefficient and incident photon energy for SR-GeSe thin films that have been deposited and annealed is presented in Fig. 4. The absorption coefficient values improved as the photon energy and annealing temperature increased.

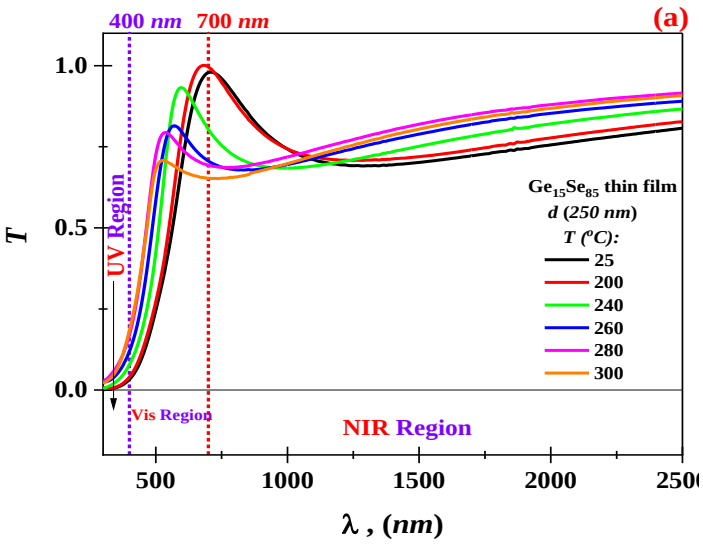

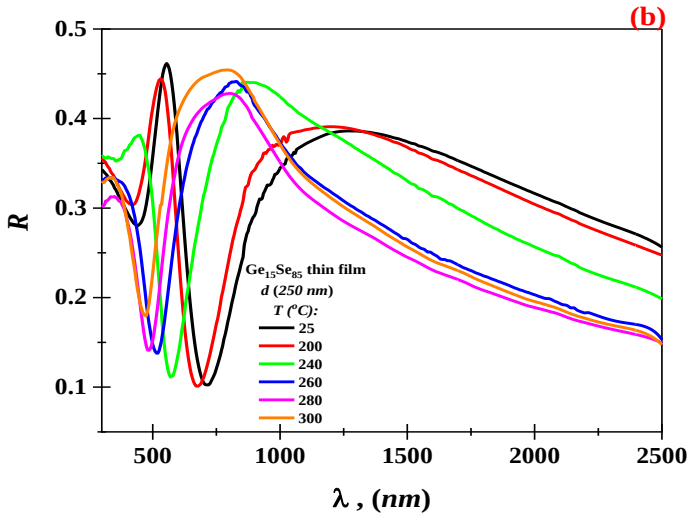

Figure 3: Mapping of Optical Spectra (*T, R*) for Pristine and Annealed SR-GeSe Thin Films

At the high absorption region ($\alpha \geq 10^4 cm^{-1}$), the linear correlation between $(\alpha h\upsilon)^{0.5}$ and $h\upsilon$ for pristine and annealed SR-GeSe thin films illustrated in Fig.5 indicates the indirect energy gap transition in SR-GeSe thin films. These findings are consistent with those obtained in the corresponding work [16]. The intercept of the extrapolations to zero absorption with the photon energy $(\alpha h\upsilon)^{0.5}=0$ could be utilized to calculate the value of E_g. The obtained E_g values are collected and listed in Table 2. According to Fig. 5, a shift in the absorption coefficient toward higher energies as a result of raising the annealing temperatures generates an increase in E_g.

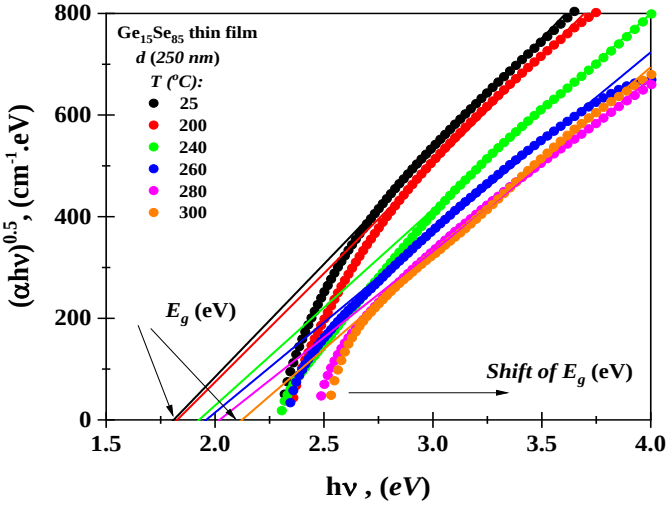

Figure 4: Diagram of Optical Absorption Coefficient for Pristine and Annealed SR-GeSe Thin Films

International Research Journal of Innovations in Engineering and Technology (IRJIET)

ISSN (online): 2581-3048

Volume 7, Issue 3, pp 36-49, March-2023

https://doi.org/10.47001/IRJIET/2023.703006

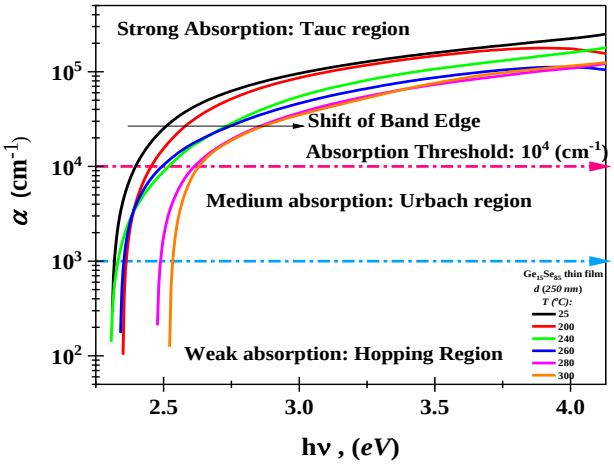

Figure 5: Computation Pathways of Energy Bandgap (Tauc Energy) According to Tauc Formula Shown in Text for Pristine and Annealed SR-GeSe Thin Films

In this work, very important methods for calculating the optical gap energy were discussed along with Tauc's method. These methods included the method of the first derivative of the transmittance as a function of wavelength. This method is inspired by a recently published work referred to in the corresponding Ref. [44]. The extraction of the optical gap energy according to this method is done by taking the values of the highest peak in the curve resulting from the derivation, as the value of the highest value in these curves indicates the optical gap energy. This method is referred to in Fig. 6 and the mentioned values for the band gap are recorded in the figure and also in Table 2.

Table 2: The Computed Values of Optical Parameters for Pristine and Annealed SR-GeSe Thin Films

$T(^{o}C)$	Optical Parameters			
	$E_g(eV)$			$E_e(eV)$
	$(\alpha h\nu)^{0.5} vs.(h\nu)$	$Max_{peak}(\frac{dT}{d\lambda})$	$Max_{peak}(R_s(\lambda))$	
25	1.802	1.750	1.747	0.114
200	1.825	1.788	1.838	0.198
240	1.921	1.912	2.085	0.245
260	1.958	2.037	2.177	0.311
280	2.017	2.106	2.298	0.339
300	2.114	2.173	2.363	0.506

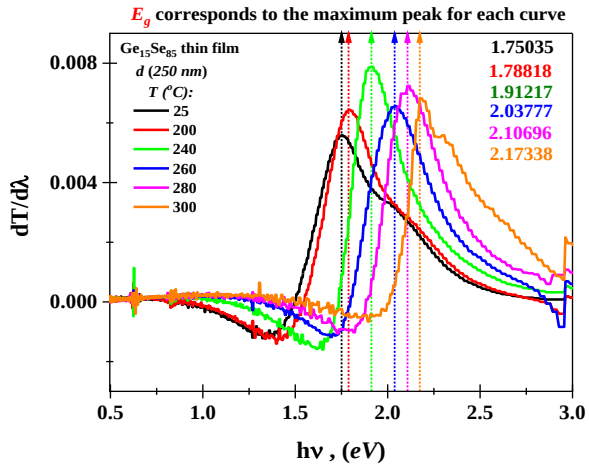

Figure 6: Computation Pathways of Energy Bandgap According to Transmittance Derivative Portrayed in Text for Pristine and Annealed SR-GeRe Thin Films

Fig. 7 shows the surface resistance behavior of pristine and annealed thin films. It is noted that the surface resistance increases with the increase of both the photon energy and the thermal annealing temperature. It is worth mentioning here that the maximum peaks at each surface resistance curve refer to the optical gap energy, which is recorded in Fig. 7 and also in Table 2.

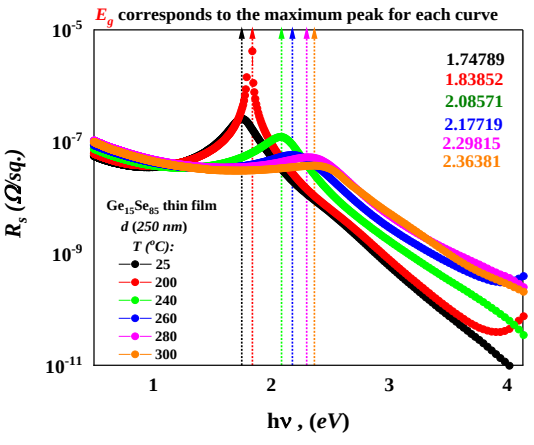

Figure 7: Computation Pathways of Energy Bandgap According to Sheet Resistance Portrayed in Text for Pristine and Annealed SR-GeSe Thin Films

International Research Journal of Innovations in Engineering and Technology (IRJIET)

ISSN (online): 2581-3048

Volume 7, Issue 3, pp 36-49, March-2023

https://doi.org/10.47001/IRJIET/2023.703006

Thin films can be used in solar cells if they are highly transparent to visible rays and electrically conductive. For this reason, we must deal with in this work a very important parameter that detects the spectral regions in which the thin film is good at passing light rays, and it is called the quality coefficient or "the figure of merit, Q". This important parameter is related to the transmittance of the thin films T and the surface resistance R_s of the thin films via Haacke equation [45]which is shown in the following formula:

$$Q = \left(\frac{T^{10}}{R_s} \right) \qquad (19)$$

Fig. 8 displays "the figure of merit, Q" parameter as a function of wavelength for the as-prepared and annealed films. It is worth mentioning here that the tracker of the spectral regions in Fig. 8will notice that the quality factor of thin films decreases in the spectral region of ultraviolet radiation and the beginning of the visible region of the spectrum, but the quality factor changes its behavior to become increasing with the increase in the degree of thermal annealing in the infrared region. Based on this harmony in the behavior of the quality of the films according to this parameter, the studied thin films can be exploited according to the desire to block or pass the light rays, and then employ them as required in modern applications [45].

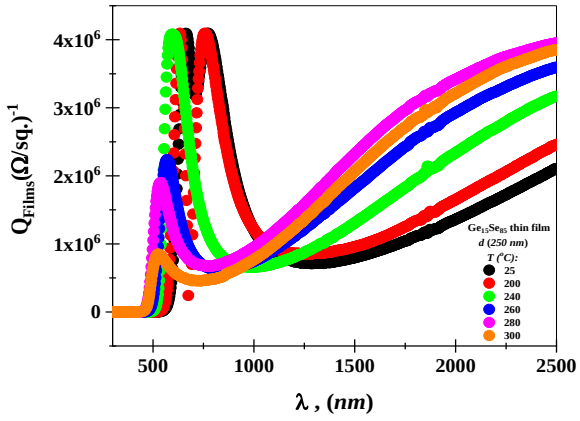

Figure 8: The Figure of Merit Pathways for Pristine and Annealed SR-GeSe Thin Films

Urbach's relation illustrated in theoretical section governs the absorption coefficient at lower photon energy in the exponential edge region where ($10^1 cm^{-1} < \alpha < 10^4 cm^{-1}$).A straight line is obtained by plotting ln(α) against the photon energy for pristine and annealed SR-GeSe thin films, as illustrated in Fig. 9. The band tail width E_e of the localized states at the band gap is given by the inverse of the slope. The computed values of E_e for studied films are listed in Table 2.The bandgap and Urbach energies (E_g, E_e) of SR-GeSe thin films exhibit opposing variations with annealing temperature. With increasing annealing temperature, the optical energy gap is widening as the width of localized states narrows. The amorphous-crystalline transitions model suggested by Mott and Davis and the density of state model can both be used to explain this phenomena [46, 47].Chalcogenide thin films typically contain substantial concentrations of unsaturated bonds or flaws. These flaws result in the localized states that are present in the amorphous band gap. Localized states in the SR-GeSe band structure are related to the Se-Se homopolar bonds (formation of uncompleted bonds) and a large number of defects. The optical band gap widens as the annealing temperature increases because there are less Se-Se homopolar bonds. The unsaturated flaws progressively soften entirely during thermal annealing at temperatures below the crystallization point, producing a huge quantity of saturated bonds. As the quantity of unsaturated defects declines, the density of localized states in the band structure drops, hence widening the optical energy gap.

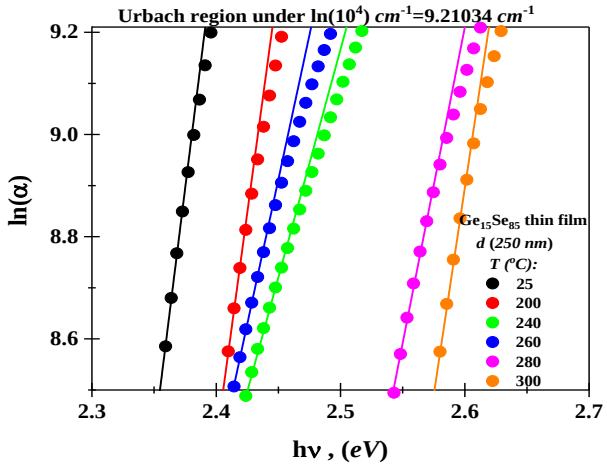

Figure 9: Computation Pathways of Urbach Energy According to Urbach Formula Incarnated in Text for Pristine and Annealed SR-GeSe Thin Films

Spectral dispersion devices and optical communication are dependent on refractive index dispersion in optical materials [48]. The values of extinction coefficient (k) and refractive index (n) were identified using the aforementioned formula in this work's theoretical section. Figs. (10, 11) illustrate the spectral dependence of extinction coefficient and refractive index for pristine and annealed SR-GeSe thin films. As the annealing temperature rises, the refractive index varies from its maximum value (n_{max}) at one wavelength to lower wavelengths. The extinction coefficient and refractive index typically decrease as annealing temperature and wavelength rise. Additionally, similar trends are seen in other semiconductor thin films [49, 50].The values of n and k drop as a result of structural and bonding configuration changes, particularly the elimination of homopolar bonds with increasing annealing temperature [51].

International Research Journal of Innovations in Engineering and Technology (IRJIET)

ISSN (online): 2581-3048

Volume 7, Issue 3, pp 36-49, March-2023

https://doi.org/10.47001/IRJIET/2023.703006

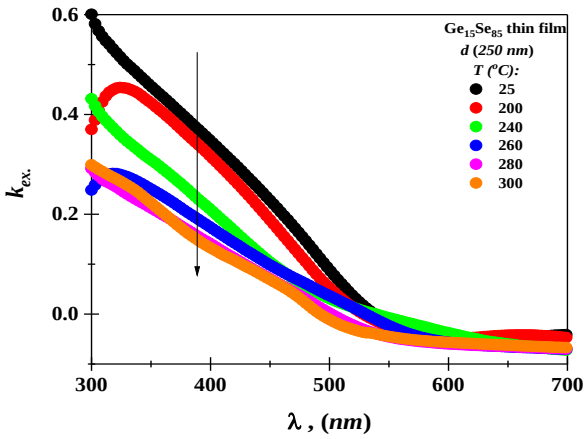

Figure 10: Extinction Coefficient Pathways for Pristine and Annealed SR-GeSe Thin Films

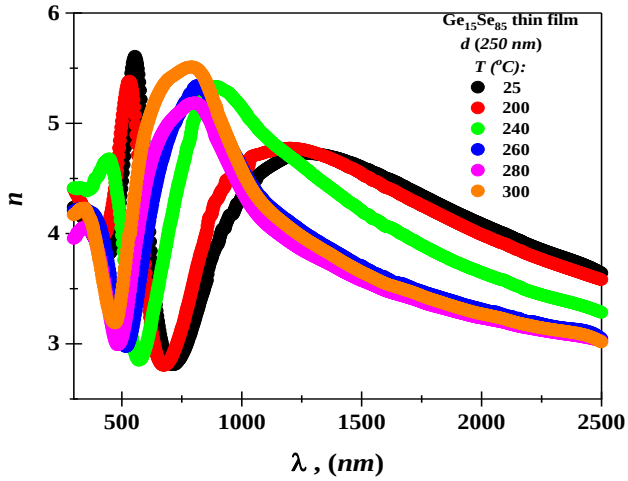

Figure 11: Refractive Index Pathways for Pristine and Annealed SR-GeSe Thin Films

Depending on the relationship between the dielectric constant and photon energy, there is an interaction between photons and electrons in films at this energy range. As a result of these interactions, the peaks in the dielectric spectra differ depending on the type of material, resulting in different shapes for the real and imaginary parts of the dielectric constant. Fig.12 portrays the relation between the real parts of the dielectric constant, ε_r, with λ^2. Straight lines were discovered to be the best way to validate Eq. (3). Higher energy curves exhibit a minor divergence from linearity, which is frequently brought on by excitonic absorption or being close to the band edge [52].

The values of N/m^*, ε_∞ and $\omega_p$can be calculated from the slopes and intercepts of the plots in Fig. 12, respectively. The values of these two parameters in correlation to the annealing temperature are listed in Table 3. It is observed that as the annealing temperature increased, N/m^*,ε_∞ and ω_p change in an identical way. Considering that the effective mass m* is constant, both decreases may be ascribed to variations in carrier concentration *N*. This has been observed in a variety of different chalcogenide systems [53-55].

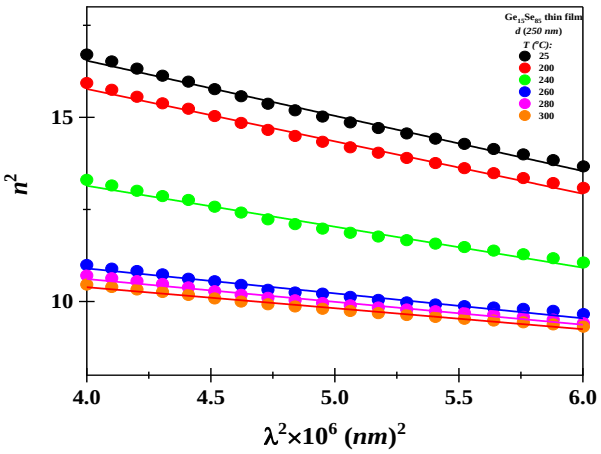

Figure 12: Extrapolation of n^2 Vs. Photon Energy for Pristine and Annealed SR-GeSe Thin Films

Based on: $n^2 = 1 + E_d E_o . \left[E_o{}^2 - (h\nu)^2 \right]^{-1}$, the plot of $(n^2\text{-}1)^{-1}$ against $(h\upsilon)^2$ for the studied thin films is shown in Fig. 13. The noticed straight line for the normal behavior with the slope $(E_oE_d)^{-1}$and the intercept with the vertical axis being E_o/E_d from which E_o and E_d may be obtained directly. Fig. 13 displays the computed values of the dispersion parameters E_o and E_d listed also in Table 3. It has been illustrated that as annealing temperatures were increased, the values of $E_o$and E_d almost increased. A common explanation for the decreased E_d with annealing temperature is that the rate of atom diffusion in the thin films has increased. As the diffusion rates rise, more atoms are deposited in interstitial locations, producing impurity-type scattering centers [56]. Furthermore, the single oscillator energy E_o=2E_g, which is in good accord with the relation of Tichá and Tich [57].

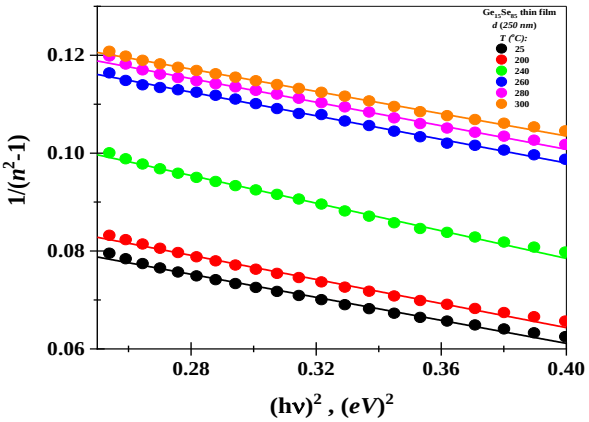

Figure 13: Extrapolation Of $1/(n^2\text{-}1)$ Vs. Photon Energy for Pristine and Annealed SR-GeSe Thin Films

International Research Journal of Innovations in Engineering and Technology (IRJIET)
ISSN (online): 2581-3048
Volume 7, Issue 3, pp 36-49, March-2023
https://doi.org/10.47001/IRJIET/2023.703006

Table 3: The Values of Dielectric and Dispersion Parameters for Pristine and Annealed SR-GeSe Thin Films

T(°C)	Dielectric Parameters			Dispersion Parameters	
	ε_∞	$N/m^* \times 10^{57}(m^{-3}.kg^{-1})$	$\omega_p \times 10^{14}(Hz)$	$E_o(eV)$	$E_d(eV)$
25	22.53	1.841	4.861	3.575	14.091
200	21.45	1.748	4.853	3.621	13.334
240	17.58	1.365	4.739	3.811	10.226
260	13.6	0.831	4.204	3.884	8.029
280	13.09	0.762	4.102	4.001	5.002
300	12.66	0.701	4.001	4.194	4.233

The importance of electronic parameters of optical materials lies in their employment in various fields of application, which include, for example, the field of solar cells, optical sensors, detectors, diodes, optical filters, display screens, alarm devices, photoelectric circuits, and so on. As a result, we calculated the energies of Plasmon Ψ, Penn E_p, and Fermi E_F mentioned in the theoretical part in this study, as well as the number of active electrons n_{eff} which are the most important electronic parameters whose behavior should be known. All values of the mentioned energies and the number of active electrons are recorded in Table 4. The behavior that dominates all these quantities is the decrease with the increase in the degree of thermal annealing. Plasma resonance frequency, which is closely associated with these quantities, can be mainly responsible for the observed decrease in these quantities [58].

Table 4: Electronic Parameters Including (Plasmon Energy ψ, Penn Energy E_P, Fermi Energy E_F and the Number of Effective Electrons n_{ff} for Pristine and Annealed SR-GeSe Thin Films

T(°C)	ψ (eV)	E_P (eV)	E_F (eV)	n_{ff} $(electron)$
25	0.32008	0.06898	0.06455	0.19786
200	0.31959	0.07067	0.06441	0.19725
240	0.31206	0.07664	0.0624	0.18807
260	0.27683	0.07799	0.05319	0.14800
280	0.27015	0.07770	0.05148	0.14095
300	0.26341	0.07714	0.04978	0.13400

Thin films' electronic polarizability is the second path that should be known in electronic parameters as it is useful in various optoelectronic applications [32, 33]. A key component of electronic polarization is polarization, which is responsible for the formation of waves within glass materials. In the form of an electron gas cloud, internal charge transfer allows electrons to travel further away from the nucleus, resulting in a total dipole moment in the network. For this reason, effective displacement must be modeled using nonlinear formula. Because solids have a wide range of applications, great efforts have been made to improve their extraction polarization ways with several formulas including that mentioned in the theoretical part. The values calculated for the electronic polarization coefficient with the formulas recorded in the theoretical part of this work are collected in Table 4.The follower of the electronic polarization behavior in Table 5 will find that the polarization values decrease with the increase in the degree of thermal annealing, which can be attributed to a large extent to the noticeable decrease in the refraction index of thin films with the increase in temperature because this is related to the increase in the scattering angles within the lattice matrix of the studied material[58].

In a related aspect, we can summarize the relationship that explains the dependence of the refractive index extracted by the theoretical methods mentioned in the theoretical part on the optical gap energy. The values of the refractive indices, or rather the refractive indexes recorded in Table 6, behave opposite to that shown by the optical gap energy, as they decrease in contrast to the increase in the optical gap energy in this work. Finally, we find that the theoretical values of the refractive index calculated in terms of the gap energy are consistent with the experimental values at the same wavelengths that correspond to the optical gap energy to a large extent, with a slight difference in each approximation and the method of calculation based on it.

International Research Journal of Innovations in Engineering and Technology (IRJIET)

ISSN (online): 2581-3048

Volume 7, Issue 3, pp 36-49, March-2023

https://doi.org/10.47001/IRJIET/2023.703006

Table 5: The Electronic Polarization α_P According Several Empirical Formulas Mentioned in Text for Pristine and Annealed SR-GeSe Thin Films

T(°C)	$\alpha_P \times 10^{-24}(cm^3)$				
	Eq.7	***Eq.8***	***Eq.9***	***Eq.10***	***Eq.11***
25	5.2758	4.7907	5.6613	5.5536	4.1818
200	5.2262	4.7805	5.6582	5.5180	4.1686
240	4.9987	4.7388	5.6456	5.3580	4.1146
260	4.6241	4.7232	5.6408	5.1106	4.0942
280	4.5592	4.6988	5.6333	5.0695	4.0620
300	4.5000	4.6600	5.6211	5.0326	4.0101

Table 6: The Refractive Index-Energy Band-Gap Dependence for Pristine and Annealed SR-GeSe Thin Films

T(°C)	n_T	n_M	n_R	n_{HV}	n_{RA}	n_{GR}	n_{RS}
25	2.97557	2.69459	2.96676	2.76671	3.00292	2.6478	2.78469
200	2.96022	2.68606	2.9525	2.75626	2.99024	2.62892	2.77333
240	2.89818	2.65185	2.89298	2.71369	2.93897	2.54844	2.72788
260	2.87512	2.63924	2.87004	2.69771	2.9199	2.51665	2.71116
280	2.83927	2.61972	2.83346	2.67271	2.89021	2.46499	2.68533
300	2.78277	2.58914	2.77332	2.63283	2.84324	2.37722	2.64498

IV. CONCLUSION

The structural and optical properties, as well as the electronic parameters of SR-GeSe thin films, were evaluated by annealing them at various temperatures. Based on X-ray diffraction results, the first and second films were amorphous while the rest films were polycrystalline. The $GeSe_2$ phase was predominantly present in the annealed polycrystalline films at 240°C to 300°C in the N_2 atmosphere along with the Se phase. The crystallite size, strain, and dislocation density were all determined from the XRD patterns. After annealing, there was a considerable drop in the films' strain and dislocation density, which suggested an increase in crystallinity. SEM images provided evidence in favor of these conclusions. The sharp absorption edge in the transmission spectrum is indicative of the SR-suitability GeSe's as filter materials. Optical absorption measurements show that the indirect band gap is what causes the absorption in both pristine and annealed thin films. While the breadth of the localized state tail narrows with increasing thermal annealing, the optical bandgap of the SR-GeSe film widens. The Davis and Mott model helps explain these findings. The refractive index dispersion data in the transmission zone were analyzed using the single-oscillator which suggested by Wemple and DiDomenico model. Using this model, the dispersion parameters were determined as functions of the annealing temperature. According to the obtained results, the heat treatment has an effects on the dispersion parameters E_d, E_o, ε_∞,and N/m^* of the studied thin films.

REFERENCES

[1] Mehta, N. "Applications of chalcogenide glasses in electronics and optoelectronics: a review." Journal of Scientific & Industrial Research, 65 (2006), 777-786.

[2] Ahluwalia, GurinderKaur, ed. "Applications of chalcogenides: S, Se, and Te." (2017): 978-3.

[3] Wei, W. H., Wang, R. P., Shen, X., Fang, L., & Luther-Davies, B. "Correlation between structural and physical properties in Ge–Sb–Se glasses." The Journal of Physical Chemistry C 117.32 (2013): 16571-16576.

[4] Solieman, Ahmed S., et al. "Dependence of optical properties on the thickness of amorphous Ge30Se70 thin films." Journal of Taibah University for Science 8.3 (2014): 282-288.

[5] Li, X., Liang, Z., Kleiner, M., & Lu, Z. L. "RTbox: A device for highly accurate response time measurements." Behavior research methods 42.1 (2010): 212-225.

[6] Alzaid, Meshal, et al. "Extraction of thickness, linear and nonlinear optical parameters of Ge20+xSe80-x thin films at normal and slightly inclined light for optoelectronic devices." Optical Materials 110 (2020): 110539.

ISSN (online): 2581-3048
Volume 7, Issue 3, pp 36-49, March-2023
https://doi.org/10.47001/IRJIET/2023.703006

[7] Alqahtani, A., et al. "Zinc-induced changes on structural pathways, optical parameters, optical constants extracted by Kramers-Kronig Formulas, Photoluminescence Spectra and photovoltaic characteristics of n-Cd50-xZnxS50/i-AgSe/p-Si solar cells." Optical Materials 134 (2022): 113055.

[8] AL-Maqate, Faisal G., et al. "Profundity study on structural and optical properties of heavy oil fly ash (HOFA) doped calcium carbonate (CaCO3) nanostructures and thin films for optoelectronic applications." Optical Materials 131 (2022): 112719.

[9] Qasem, Ammar, et al. "Adapting the structural, optical and thermoelectrical properties of thermally annealed silver selenide (AgSe) thin films for improving the photovoltaic characteristics of the fabricated n-AgSe/p-CdTe solar cells." Journal of Alloys and Compounds 899 (2022): 163374.

[10] Alshahrani, B., et al. "The Pivotal Role of Thermal Annealing of Cadmium Telluride Thin Film in Optimizing the Performance of CdTe/Si Solar Cells." Journal of Electronic Materials 50.8 (2021): 4586-4598.

[11] Elsaeedy, H. I., et al. "The significant role of ZnSe layer thickness in optimizing the performance of ZnSe/CdTe solar cell for optoelectronic applications." Optics & Laser Technology 141 (2021): 107139.

[12] Liu, Shun-Chang, et al. "GeSe thin-film solar cells." Materials Chemistry Frontiers 4.3 (2020): 775-787.

[13] Chen, Binwen, et al. "Magnetron sputtering deposition of GeSe thin films for solar cells." Solar Energy 176 (2018): 98-103.

[14] Pandey, V., S. K. Tripathi, and A. Kumar. "Effect of in incorporation on optical properties of amorphous Se–Ge thin films." Physica B: Condensed Matter 388.1-2 (2007): 200-205.

[15] Bakr, N., M. Aziz, and M. Hammam. "Structural properties of GexSe1-x thin films prepared by semi-closed space technique." Egypt J Sol 23 (2000): 45.

[16] Alnajjar, AbdallaAbdelaziz. "The role of thermal treatment on the optical properties of Ge0.15Se0.85 system." Renewable energy 34.1 (2009): 71-74.

[17] M. Rashada, A. Mossad Ali, H.H. Somaily, H. Algarnl, D. Hamad, A.A. Hendid and M.M. Hafiz. "Microwave irradiation effects on structural and optical investigations of nanostructured Ge25Se75 glassy films" Acta Physica Polonica A, 138 (2020). 434-439.

[18] S.I. Qashou, A.M. Ali, H.H. Somaily, H. Algarn, M.M. Hafiz, M. Rashad, "Linear and nonlinear optical investigations of Ge25Se75 thin films at different annealing temperatures", Physica B: Physics of Condensed Matter (2021), doi: https://doi.org/10.1016/j.physb.2021.413351.

[19] Alqahtani, A., et al. "A profound analysis of structural, thermal, optical, and electrical properties of Cd50Pb30S20 composition for optoelectronic devices: implications of changes in film's thickness." Optical and Quantum Electronics 55 (2023): 18.

[20] Qasem, Ammar, et al. "Determination of optical bandgap energy and optical characteristics of Cd30Se50S20 thin film at various thicknesses." Optics & Laser Technology 148 (2022): 107770.

[21] H. Mahfoz Kotb, M.A. Dabban, F.M. Abdel-Rahim, A.Y. Abdel-latif, M.M. Hafiz, "Thermally induced effects on structural and electrical properties of selenium-rich Cd-Se thin films", Physica B: Condensed Matter, 406 (2011) 1326-1329.

[22] H. Mahfoz Kotb, M.A. Dabban, A.Y. Abdel-latif, M.M. Hafiz, "Annealing temperature dependence of the optical and structural properties of selenium-rich Cd-Se thin films", Journal of Alloys and Compounds, 512 (2012), 115-120.

[23] El-Korashy, A., H. El-Zahed, and M. Radwan. "Optical studies of [N (CH3)4]2CoCl4,[N (CH3) 4]2MnCl4 single crystals in the normal paraelectric phase." Physica B: Condensed Matter 334.1-2 (2003): 75-81.

[24] Ahmed, Moustafa, et al. "The main role of thermal annealing in controlling the structural and optical properties of ITO thin film layer." Optical Materials 113 (2021): 110866.

[25] Naim, Abdullah FAL, et al. "The main role of bismuth in controlling linear and nonlinear optical, electronic and electrical parameters of Se–Ge–Bi thin films." Journal of Materials Science: Materials in Electronics 32.6 (2021): 6866-6882.

[26] Abdulnasser Alfaqeer, Ahmed lrebati, Mehdi Dabban, "Extraction of Optical Constants and Dispersion Parameters of CdTe/CdSe Bi-Layer Thin Films" The scientific Journal of university of Saba region, Vo. 5 No. 1 -December 2022.

[27] Shaaban, E. R., et al. "Investigation of Structural and Optical Properties of Amorphous-Crystalline Phase Transition of As40S45Se15 Thin Films."Acta Physica Polonica, A. 136.3 (2019).

[28] Shaaban, Essam R., et al. "Optical constants, dispersion parameters and non-linearity of different thickness of As40S45Se15 thin films for optoelectronic applications." Optik 186 (2019): 275-287.

[29] Soraya, M. M., et al. "Indium incorporation effects on optical properties of quaternary chalcognide Se-Zn-Te-In films." Chalcogenide Letters 17.3 (2020): 133-145.

[30] Kumar, V., and B. S. R. Sastry. "Heat of formation of ternary chalcopyrite semiconductors." Journal of Physics and Chemistry of Solids 66, no. 1 (2005): 99-102.

ISSN (online): 2581-3048
Volume 7, Issue 3, pp 36-49, March-2023
https://doi.org/10.47001/IRJIET/2023.703006

[31] Phillips, J. C. "Bonds and Bands in Semiconductors (Academic Press, New York, 1973).".

[32] Gupta, V. P., V. K. Srivastava, and P. N. L. Gupta. "Electronic properties of chalcopyrites." Journal of Physics and Chemistry of Solids 42, no. 12 (1981): 1079-1085.

[33] Reddy, R. R., Y. Nazeer Ahammed, K. Rama Gopal, P. Abdul Azeem, T. V. R. Rao, and P. Mallikarjuna Reddy. "Optical electronegativity, bulk modulus and electronic polarizability of materials." Optical Materials 14, no. 4 (2000): 355-358.

[34] El-Nahass, M. M., and A. A. M. Farag. "Structural, optical and dispersion characteristics of nanocrystalline GaN films prepared by MOVPE." Optics & Laser Technology 44, no. 2 (2012): 497-503.

[35] R.L.Sutherland, D.G.Mclean, S.Kikparik, Handbook on Non-Linear optics second ed, Marcel Dekkar inc, New York, (2003).

[36] Duffy, J. A. "Trends in energy gaps of binary compounds: an approach based upon electron transfer parameters from optical spectroscopy." Journal of Physics C: Solid State Physics 13, no. 16 (1980): 2979.

[37] Tripathy, S. K. "Refractive indices of semiconductors from energy gaps." Optical materials 46 (2015): 240-246.

[38] Moss, T. S. "A relationship between the refractive index and the infra-red threshold of sensitivity for photoconductors." Proceedings of the Physical Society. Section B 63.3 (1950): 167.

[39] Ravindra, N. M., Sushil Auluck, and V. K. Srivastava. "On the Penn gap in semiconductors." Physica status solidi (b) 93.2 (1979): K155-K160.

[40] Herve, P., and L. K. J. Vandamme. "General relation between refractive index and energy gap in semiconductors." Infrared physics & technology 35.4 (1994): 609-615.

[41] Herve, P. J. L., and L. K. J. Vandamme. "Empirical temperature dependence of the refractive index of semiconductors." Journal of Applied Physics 77.10 (1995): 5476-5477.

[42] Reddy, R. R., S. Anjaneyulu, and C. L. N. Sarma. "Relationship between energy gap, refractive index, bond energy and the szigeti charge in polyatomic binary compounds and semiconductors." Journal of Physics and Chemistry of Solids 54.5 (1993): 635-637.

[43] Gupta, V. P., and N. M. Ravindra. "Comments on the moss formula." physica status solidi (b) 100.2 (1980): 715-719.

[44] Qasem, Ammar, et al. "Tunability of structural, optical, and electrical properties of pristine MnSe thin film by gradually changing temperature for optoelectronic applications." Physica B: Condensed Matter 627 (2022): 413600.

[45] Haacke, G. "New figure of merit for transparent conductors." Journal of Applied Physics 47.9 (1976): 4086-4089.

[46] Khan, M. I., et al. "Structural, morphological, electrical and optical properties of Cu doped DLC thin films." Materials Research Express 6.12 (2019): 126420.

[47] Victoria, S. Grace, A. Moses Ezhil Raj, and C. Ravidhas. "An insight in the structural, morphological, electrical and optical properties of spray pyrolysed Co3O4 thin films." Materials Chemistry and Physics 162 (2015): 852-859.

[48] He, Chongjun, et al. "Optical transmission and dispersion of 0.25 Pb (In1/2Nb1/2) O3–(0.75−x) Pb (Mg1/3Nb2/3) O3–x PbTiO3 single crystals." Journal of Applied Physics 117.16 (2015): 164104.

[49] Moussa, N. M., et al. "Chromium doped ZnO nanoparticles for energy storage, gas and humidity sensing and spin based electronic devices applications." Optical and Quantum Electronics 54.11 (2022): 1-20.

[50] Elsaeedy, H. I., et al. "The pivotal role of TiO2 layer thickness in optimizing the performance of TiO2/P-Si solar cell." Journal of Alloys and Compounds 867 (2021): 159150.

[51] Kincl, M., and L. Tichý. "Thermally and optically induced irreversible changes in some Ge–As–S amorphous thin films." Materials Chemistry and Physics 110.2-3 (2008): 322-327.

[52] Gadalla, A., et al. "Optical constants and dispersion parameters of amorphous Se65− xAs35Sbx thick films for optoelectronics." Indian Journal of Physics 95.9 (2021): 1853-1863.

[53] Fouad, S. S., A. E. Bekheet, and A. M. Farid. "Derivation of a relation between the conduction mechanism and chemical bonding of amorphous Ge15Se85−xAgx alloys." Physica B: Condensed Matter 322.1-2 (2002): 163-172.

[54] E. Marquez, J. M. Gonzalez-Leal, A. M. Bemal-Oliva, R. Jimenez –Garay and T. Wagner J. Non-Cryst. Solids 354 (2008) 503.

[55] Yakuphanoglu, F., and C. Viswanathan. "Electrical conductivity and single oscillator model properties of amorphous CuSe semiconductor thin film." Journal of non-crystalline solids 353.30-31 (2007): 2934-2937.

[56] Qasem, Ammar, et al. "Extraction of thermal and optical parameters for As–Se–Te thin films according to phase-change pathways." Materials Chemistry and Physics 277 (2022): 125620.

[57] Ticha, H., and L. Tichy. "Semiempirical relation between non-linear susceptibility (refractive index), linear refractive index and optical gap and its

ISSN (online): 2581-3048
Volume 7, Issue 3, pp 36-49, March-2023
https://doi.org/10.47001/IRJIET/2023.703006

application to amorphous chalcogenides." J. Optoelectron. Adv. Mater 4.2 (2002): 381-386.

[58] Qasem, Ammar, et al. "Optical and electronic properties for As-60 at % S uniform thickness of thin films: Influence of Se content." Optical Materials 109 (2020): 110257.

Citation of this Article:

Mehdi Ahmed Dabban, Tawfik Mahmood Mohammed Ali, Abdel-naser A. M. Alfaqeer, "Major Role of Annealing Temperature Effect on the Structural Pathways, Optical Properties, Sheet Resistance, Quality Factor, and Electronic Parameters of Selenium-Rich $Ge_{15}Se_{85}$ Pristine Thin Film for Optoelectronic Applications" Published in *International Research Journal of Innovations in Engineering and Technology - IRJIET*, Volume 7, Issue 3, pp 36-49, March 2023. Article DOI https://doi.org/10.47001/IRJIET/2023.703006

****

